Battery internal temperature estimation by combined impedance and surface temperature measurement

CrossMark

Robert R. Richardson, Peter T. Ireland, David A. Howey*

Department of Engineering Science, University of Oxford, Oxford, UK

HIGHLIGHTS

- Method introduced for estimating cylindrical Li-ion cell temperature distribution.
- Impedance measurement alone shown to underestimate maximum internal temperature.
- The new method combines impedance with surface temperature measurements.
- Method validated experimentally for the first time with an internal thermocouple.
- The method is efficient enough to be implemented in a battery management system.

ARTICLE INFO

ABSTRACT

A new approach, suitable for real-time implementation, is introduced for estimation of non-uniform internal temperature distribution in cylindrical lithium-ion cells. A radial 1-D model is used to estimate the distribution using two inputs: the real or imaginary part of the electrochemical impedance of the cell at a single frequency, and the surface temperature. The approach does not require knowledge of cell thermal properties, heat generation or thermal boundary conditions.

The model is validated experimentally, the first time for such an approach, using a cylindrical 26650 cell fitted with an internal thermocouple. The cell is heated by applying (1) current pulses of up to ± 20 A and (2) a 3500 s HEV drive cycle current profile, whilst monitoring the surface and core temperatures and measuring impedance at 215 Hz. During the drive cycle test, the battery core temperature increases by 20 °C and the surface temperature increases by 14 °C. The mean absolute error in the predicted maximum temperature throughout the cycle is 0.6 °C (3% of the total core temperature increase), in contrast to a mean absolute error of 2.6 °C if the temperature is assumed to be uniform (13% of the total core temperature increase).

© 2014 Elsevier B.V. All rights reserved.

1. Introduction

The use of lithium ion batteries for energy storage in automotive and aerospace applications has led to larger cell sizes and the requirement for more aggressive charging and discharging. Under typical operating conditions, such as a standard HEV drive cycle, cells may experience temperature differences between surface and core of 10 °C or more [1]. The ability to estimate the temperature distribution during operation, including the maximum temperature, is necessary for battery management systems (BMS) for safety and control purposes. High battery temperatures could trigger thermal runaway resulting in problems such as fires, venting, and electrolyte leakage. While such incidents are rare (occurring in one in 1 million to one in 10 million batteries [2]), consequences include costly recalls and potential endangerment of human life. Consequently, the ability to estimate internal temperature gradients and maximum temperatures in batteries during operation is vital.

Existing battery management systems typically use a temperature sensor mounted to the surface of the cell and equate the measured temperature to the cell mean temperature. An improved estimate of cell internal temperature can be made by using a lumped-parameter thermal model [1,3–5] or an approximate distributed thermal model [6,7]. However, these suffer from a

* Corresponding author. Room 15.10, Holder Building, Department of Engineering Science, University of Oxford, Parks Road, Oxford OX1 3PJ, UK. Tel.: +44 1865 283 476; fax: +44 1865 273 010.
E-mail addresses: robert.richardson@eng.ox.ac.uk (R.R. Richardson), peter.ireland@eng.ox.ac.uk (P.T. Ireland), david.howey@eng.ox.ac.uk (D.A. Howey).

number of drawbacks: Firstly, it is difficult to estimate the required model parameters, such as heat generation and cell thermal properties. The heat generation term is normally approximated as the product of the current squared, I^2, and the internal resistance, R_e. The value of R_e is difficult to estimate since it is a function of temperature, state of charge (SOC) and state of health (SOH). The thermal properties of the cell are also difficult to measure, since cells consist of many different materials combined into a layered structure, and there are unknown thermal contact resistances between the layers [8]. A second inherent problem is that rapid fluctuations in internal temperature may not be registered by surface mounted temperature sensors, regardless of the sampling frequency. This may mean thermal runaway cannot be detected, since associated timescales are often shorter than timescales associated with heat conduction through the cell [9]. Consequently, surface mounted temperature sensors even when used with a thermal model may be insufficient to track internal temperature or predict thermal runaway.

One approach to overcome these problems is to embed micro-temperature sensors within the cell [10,11]. However, the additional manufacturing challenges and instrumentation requirements of this approach would significantly increase cost and complexity.

As an alternative approach, Srinivasan et al. [12,13] demonstrated temperature estimation between −20 and 66 °C based on electrochemical impedance, specifically phase of impedance at a single frequency between 40 and 100 Hz. This frequency range was chosen since it is temperature sensitive but insensitive to other parameters such as SOC and SOH. Srinivasan assumed that internal cell temperature is uniform, whereas under typical operating conditions cells exhibit large internal temperature non-uniformities and the estimated temperature may differ greatly from the true maximum temperature as we demonstrate in this paper.

The effect of temperature non-uniformity on electrochemical impedance was studied by Troxler et al. [14] who showed that the effective impedance of a cell with a temperature gradient applied could be accurately modelled by treating the cell as a parallel electrical connection of individual electrodes. Schmidt et al. [15] show that this approach can be used for accurate sensorless estimation of mean internal temperature in a prismatic cell.

2. Thermal-impedance model

The literature previously discussed shows that impedance may be used to estimate cell mean temperature. However, in practice there may be a significant difference between internal maximum temperature, surface temperature and mean temperature, particularly in cylindrical cells under heavy loading conditions. We therefore address this by developing a thermal-impedance model which estimates the temperature distribution by combining an electrochemical impedance spectroscopy (EIS) measurement at a single frequency with a surface temperature measurement.

Previous studies have used as a temperature-dependent parameter the real part of the impedance at a specific frequency [15], the phase shift at a specific frequency [12,13], and the intercept frequency [16]. To demonstrate our technique, we use the real part of the impedance at 215 Hz.

The model is for cylindrical cells, since these exhibit the largest temperature gradients [17], although a similar analysis could be applied to prismatic cells. The model is one-dimensional in the radial direction and assumes negligible heat loss through the ends of the cell. This condition is valid for cells connected in series with identical cells on either end [18], a configuration which may apply to the majority of cells in a large battery pack.

The impedance of a cell depends on the temperature distribution throughout the cell active material. We define $T_{uniform}$ as the uniform cell temperature that would give rise to the measured impedance. However, there are an infinite number of temperature distributions that could give rise to any given impedance measurement, and so $T_{uniform}$ is only representative of the actual cell temperature when the cell temperature is in fact uniform. By using an additional surface temperature measurement in combination with the impedance measurement, and by assuming a quadratic radial temperature distribution based on the solution of a steady-state thermal model, the true internal temperature distribution, and consequently the maximum internal temperature, may be estimated.

2.1. Electrochemical impedance for non-uniform temperature distributions

The principle of EIS is to apply a small single-frequency sinusoidal current signal and measure the voltage response from a cell, which depends on the impedance. The impedance, Z, is the transfer function of the voltage U with respect to the current I:

$$Z(j\omega) = \frac{U(j\omega)}{I(j\omega)} = Z'(\omega) + jZ''(\omega) \tag{1}$$

with $j\omega = j2\pi f$, where j is the imaginary number and f is the frequency, and Z' and Z'' are the real and imaginary parts of the impedance, respectively. The inverse of cell impedance is the admittance, given by

$$G(j\omega) = \frac{1}{Z(j\omega)} = G'(\omega) + jG''(\omega) \tag{2}$$

Since admittances in parallel are additive, it is more straightforward to use admittance than impedance in the following analysis. The specific admittance (or admittivity), denoted g in this study, is the admittance per unit volume, in analogy to conductance and conductivity in a resistive circuit. If the admittance throughout a cell is uniform, the admittivity is given by

$$g(j\omega) = \frac{G(j\omega)}{V} = g'(\omega) + jg''(\omega) \tag{3}$$

where V is the volume (or sub-volume) of interest and $g'(\omega)$ and $g''(\omega)$ are the real and imaginary parts of the local admittivity respectively. A cylindrical cell with a continuous temperature distribution in the radial direction is equivalent to an infinite number of concentric annuli, each of which has radius r, thickness dr, and length L, as shown in Fig. 1.

Since admittivity varies with temperature (as discussed below), the admittance of each infinitesimal annulus depends on the temperature at that radius. Since each of the elements are electrically connected in parallel, and admittances in parallel are additive, the admittance of the entire cell is therefore:

$$G(j\omega) = \int_V g(r, j\omega)dV \tag{4}$$

provided that the admittivity varies in the radial direction only. This assumption is valid if the heat transfer from the top and bottom ends of the cell is negligible, and is often approximately true for cylindrical cells, since the tabs connecting the active material to the casing at either end have small cross sections, giving rise to relatively high thermal resistances compared to the radial path [17]. Substituting V with $\pi(r_o^2 - r_i^2)L$ and dV with $2\pi Ldr$, and simplifying, yields
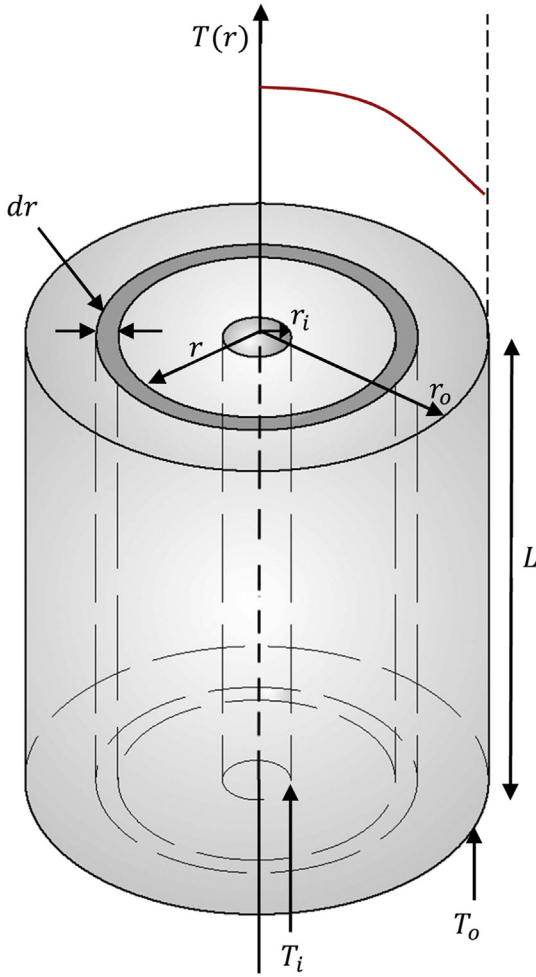
Fig. 1. The cell jelly-roll with a continuous temperature distribution in the radial direction modelled as an infinite number of radially arranged volumetric elements of radius r, thickness dr, and length L.

$$G(j\omega) = 2\pi L \int_{r_i}^{r_o} rg(r, j\omega)dr \tag{5}$$

where r_i and r_o are the inner and outer radii of the cell active material. It follows that the real part of the admittance at a single frequency is related to the real part of the admittivity at that frequency by

$$G'_{\omega_1} = 2\pi L \int_{r_i}^{r_o} rg'_{\omega_1}(r)dr \tag{6}$$

where the subscript ω_1 denotes admittance at the frequency ω_1. The relationship between G'_{ω_1} and uniform cell temperature can be approximated by a second order polynomial fit from experimental data[1]:

$$G'_{\omega_1} = a + bT_{\text{uniform}} + cT^2_{\text{uniform}} \tag{7}$$

where T_{uniform} is the uniform cell temperature and a and b are the fitting coefficients. Note that Eq. (7) is only valid when the cell temperature is actually uniform and G'_{ω_1} is a monotonic function of T in the range of interest, which is the case in the present study. By extension, similar relationships exist for other impedance parameters (such as the imaginary part of impedance, the phase shift etc.), and so these could equally be used as the impedance-based inputs to the model.

The admittivity is then related to the local radially resolved temperature by

$$g'_{\omega_1} = \frac{a + bT(r) + cT^2(r)}{V} \tag{8}$$

Substituting (8) into (6), replacing V with $\pi(r_o^2 - r_i^2)L$, and rearranging, gives an expression relating the measured admittance to the temperature distribution

$$G'_{\omega_1} = \frac{2}{r_o^2 - r_i^2} \int_{r_i}^{r_o} r\left(a + bT(r) + cT^2(r)\right)dr \tag{9}$$

The term on the left hand side of this equation is the overall cell admittance at the selected frequency, ω_1, which is measured in real time. To estimate the temperature distribution in the cell, the above expression alone is not sufficient, since there are an infinite number of temperature distributions that could give rise to a given measured admittance. Therefore, a simple thermal model is used to constrain the solution as discussed in the next section.

2.2. Steady-state thermal model

The thermal behaviour of a cell is modelled using a steady state solution of the one-dimensional cylindrical heat equation with uniform heat generation throughout the active material. The steady-state assumption is chosen as it gives rise to a unique analytical solution which results in an efficient numerical model which could be solved in real time in a BMS. In reality, the cell does not always operate in steady-state, since both the internal heat generation and the environmental temperature conditions may vary with time. In this paper the environmental temperature conditions were held constant during transient tests, but the heat generation was varied according to a drive cycle. It is shown in Section 4 by experimental validation against an internal thermocouple that the effect of the steady-state assumption is to introduce an error during transient periods, however this is relatively small, and even during a dynamic drive cycle the predicted and measured maximum temperatures remain in good agreement.

The one-dimensional steady-state solution to the heat equation for an annulus with uniform heat generation is ([19]):

$$T(r) = T_o + \frac{\dot{q}r_o^2}{4k}\left(1 - \frac{r^2}{r_o^2}\right) \\ - \left[\frac{\dot{q}r_o^2}{4k}\left(1 - \frac{r_i^2}{r_o^2}\right) + (T_o - T_i)\right]\frac{\ln(r_o/r)}{\ln(r_o/r_i)} \tag{10}$$

At the inner surface of the active material, the rate of heat flow will be zero at steady-state, since the central mandrel does not generate heat. The temperature distribution can therefore be obtained as a function of r and the parameters r_i, r_o, T_i and T_o only (i.e. it is independent of $\dot{q}$ and k). By differentiating Eq. (10) with respect to r, to obtain dT/dr, and setting $q_i'' = 0$ at $r = r_i$, the following boundary condition for the heat flux at the inner surface is obtained:

$$q_i'' = \frac{\dot{q}r_i}{2} - \frac{k\left[\frac{\dot{q}r_o^2}{4k}\left(1 - \frac{r_i^2}{r_o^2}\right) + (T_o - T_i)\right]}{r_i \ln(r_o/r_i)} = 0 \tag{11}$$

By solving both Eqs. (10) and (11) for $\dot{q}/k$, and equating the results, an expression for the temperature distribution, $T(r)$, which is independent of $\dot{q}$ and k, is obtained:

$$T(r) = T_o + \left(\frac{C_i r_o^2}{4}\right)\left(1 - \frac{r^2}{r_o^2}\right) \\ - \left[\left(\frac{C_i r_o^2}{4}\right)\left(1 - \frac{r^2}{r_o^2}\right) + (T_o - T_i)\right]\frac{\ln(r_o/r)}{\ln(r_o/r_i)} \tag{12}$$

Where

$$C_i = \frac{4(T_i - T_o)}{r_o^2 - r_i^2(2\ln r_o/r_i) + 1} \tag{13}$$

2.3. Combined thermal-impedance model

Substituting the solution for $T(r)$ (Eq. (12)) into the solution for the measured impedance (Eq. (9)), and integrating with respect to r over the interval r_i to r_o, gives an equation which relates measured cell admittance, G_{ω_1}, to the parameters r_i, r_o, T_i and T_o. The only unknown parameter in this equation is T_i, the maximum temperature at the inner surface of the jelly roll. This simplifies to a quadratic equation of the form

$$AT_i^2 + BT_i + C = 0 \tag{14}$$

where A and B are terms containing r_i and r_o (which are known a priori), and T_o and G_{cell} (which are measured in real time).

An overview of the full procedure is outlined in Fig. 2. Although this technique relies on a number of approximations, it has the potential to yield an accurate estimation of maximum internal temperature for inputs based on typical HEV drive cycles as demonstrated in Section 4.2. Furthermore, since the only measurements required are the single frequency impedance and the surface temperature, and the thermal model is not computationally intensive, the entire procedure could be carried out in an online BMS.

3. Experimental setup

In order to demonstrate the technique on a real cell, experiments were carried out with a 2.3 Ah cylindrical cell (A123 Model ANR26650 m1-A) with LiFePO$_4$ cathode and a graphite anode. The properties of the cell are given in Table 1. The cell was fitted with two thermocouples, one on the surface and another inserted into the core via a hole which was drilled in the positive electrode end. Cell cycling and impedance measurements were carried out using a Biologic HCP-1005 potentiostat/booster. The impedance was measured using Galvanostatic Impedance Spectroscopy (GEIS) with a 200 mA peak-to-peak perturbation current. The environmental temperature was controlled with a Votsch VT4002 thermal chamber.

3.1. Calibration

In order to calibrate the impedance against temperature, EIS measurements were conducted on the cell in thermal equilibrium conditions over a temperature range of −20 °C to +45 °C in intervals of 5 °C, and over a range of 10–90% SOC in intervals of 20%. The EIS frequency range spanned 1 kHz to 1 Hz with 10 frequencies
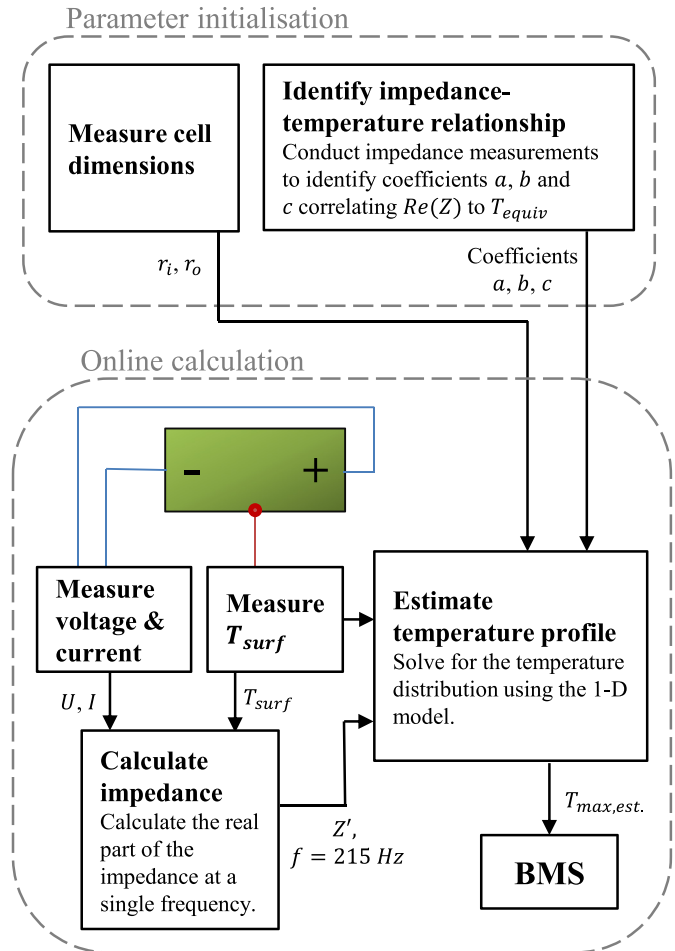

Fig. 2. Process flowchart for real-time estimation of cell internal temperature distribution.

per decade and 3× averaging. The cell capacities at each temperature were first determined with a constant current constant voltage (CCCV) charge/discharge. The SOC was then adjusted to the required values by drawing a 0.9C current. At each SOC, the cell was allowed to rest to ensure its temperature had equilibrated, which typically occurred in less than 2 h. This was verified when the temperatures registered by the internal and surface thermocouples were within 0.2 °C and repeated impedance measurements over a 20 min period yielded identical results.

3.2. Validation

Validation experiments consisted of applying (1) symmetrical current pulses and (2) a HEV drive cycle to the cell whilst single frequency (215 Hz) impedance measurements were carried out periodically and the surface and internal temperatures were

Table 1
Properties of the lithium ion cell used for validation.

Model	A123 ANR26650 m1-A
Anode material	Graphite
Cathode material	LiFePO$_4$
Nominal voltage	3.3 V
Nominal capacity	2.3 Ah
Cell housing length	65 mm
Cell outer diameter	26 mm

monitored. This frequency was selected based on the analysis of the full spectrum impedance results as discussed in Section 4.1. In order to minimize heat loss through the cell ends, they were insulated using Styrofoam (Fig. 3). Before each experiment, the SOC was adjusted to 50% by drawing a 0.9C current. The temperature of the thermal chamber was set to 8 °C and the cell was allowed to rest until its temperature equilibrated.

Besides being a function of temperature and SOC, the impedance is also a function of DC current, mainly due to the charge transfer polarization decreasing with increasing current [20]. Preliminary results confirmed that when the EIS perturbation current is superposed over an applied current load (e.g. the current pulses or drive cycle), the impedance measurement is altered. To overcome this, the cell was allowed to rest for 4 s before each EIS measurement was taken. The duration of this rest period was kept as short as possible to ensure that the thermal response of the cell to the applied cycle was not significantly altered, and it was found that the core cell temperature dropped by at most 0.25 °C during any one of these rest periods. In practice, it may be possible to carry out impedance measurements during natural rest periods in a drive cycle, however, the issue of impedance measurement under load warrants further investigation.

In the current pulse experiments, symmetric and periodic current pulses with 0.03 Hz frequency and magnitudes of ±10 A and ±20 A were applied. Single frequency impedance measurements were taken between each current pulse. The current pulses were maintained until the battery internal temperature reached an approximate steady state. After this time, the current was switched off to allow for temperature relaxation, and the impedance measurements continued to be taken every 60 s, until the temperature of the cell had equilibrated with the temperature of the chamber. In the HEV drive cycle experiment, a 3500 s portion of an Artemis drive cycle was applied to the cell and EIS measurements were taken every 24 s, i.e. 20 s periods of the drive cycle followed by 4 s rests.

4. Results & discussion

4.1. Impedance measurements

Fig. 4 shows an example impedance spectrum at a uniform cell temperature of 10 °C, and various states of charge, over the frequency range 1 Hz to 1 kHz. It can be seen from this figure that the impedance at $f > 100$ Hz is approximately independent of SOC at this temperature, for this particularly battery chemistry. The frequency for temperature evaluation was chosen to be 215 Hz, since
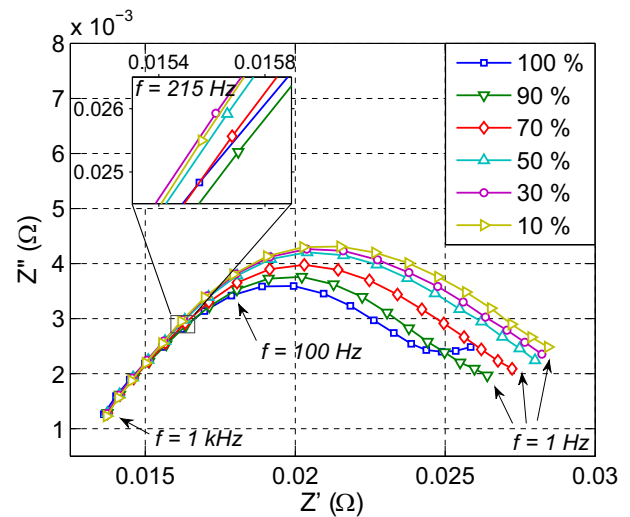

Fig. 4. Impedance at 10 °C and various states of charge between 2 kHz and 1 Hz. Inset: Impedance at $f = 215$ Hz. Above this frequency the real part of the impedance is approximately independent of SOC.

variation with SOC is observed at lower frequencies while at higher frequencies the variation of impedance with temperature decreases (see Fig. 5). Similar behaviour is exhibited at the other investigated temperatures such that the uncertainty in temperature predicted due to variation in SOC is never greater than 2 °C. Therefore subsequent results focus on the 50% SOC behaviour only.

Fig. 5 shows the full impedance spectrum at 50% SOC over the temperature range −20 to 45 °C. Both the real and imaginary impedance vary by an order of magnitude over this temperature range, demonstrating the high sensitivity of impedance to temperature in this range.

Fig. 6 shows a Bode plot of the impedance at 50% SOC. It is evident that both the real and imaginary impedance decrease consistently as temperature is increased at all frequencies, including at $f = 215$ Hz. It is also evident that toward the high end of the temperature range, the variation of impedance with temperature decreases. However, up to temperatures of 45 °C the impedance monotonically increases with temperature.

The real impedance is expected to have an Arrhenius dependence on temperature, of the form:

$$Z^{'}(T) = k.\exp\left(\frac{E_a}{RT}\right) \qquad (15)$$

where k is a constant, E_a is the activation energy and R is the Universal gas constant. Similar to [15], the electrical conductivity of the current collector was considered as constant over the investigated temperature range and so a constant resistance R_{col} was subtracted from the measured real impedance $Z^{'}_{meas}$ in order to obtain the active material impedance Z':

$$Z'(T) = Z'_{meas}(T) - R_{col} \qquad (16)$$

The resulting cell impedance and Arrhenius fit are shown in Fig. 7, whilst Fig. 8 shows a plot of the real admittance against temperature. In addition to an Arrhenius fit, this plot includes a quadratic polynomial fit directly to the admittance of the active material, $Y'(T) = 1/Z'(T)$. Both fits show good agreement with the experimental data ($R^2 > 0.99$ for each), however the polynomial fit was used in the present model for computational convenience, as previously discussed. The coefficients of the fitted polynomial are
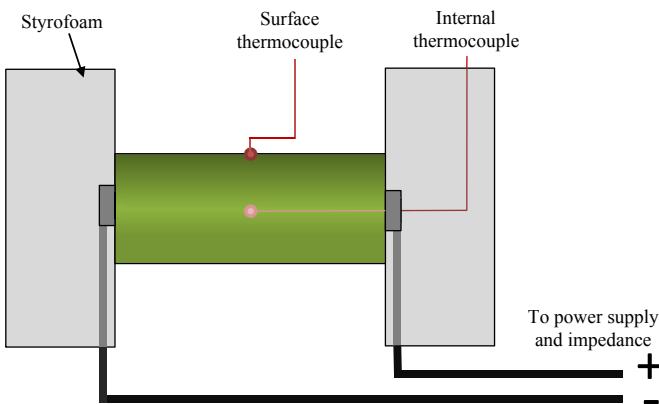

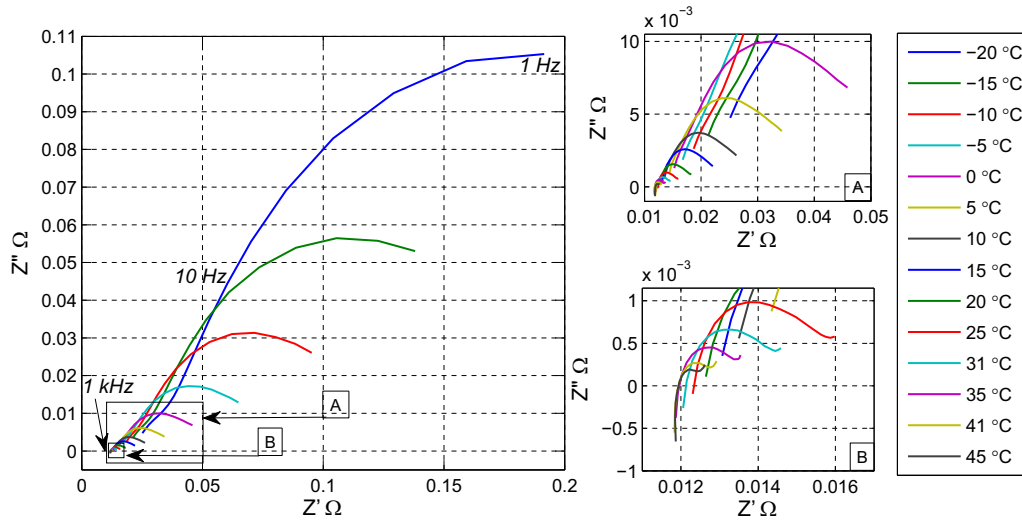**Fig. 3.** Experimental setup for validation of the predicted maximum cell temperature.

Fig. 5. Impedance at 50% SOC at various temperatures over the frequency range 1 Hz–2 kHz.
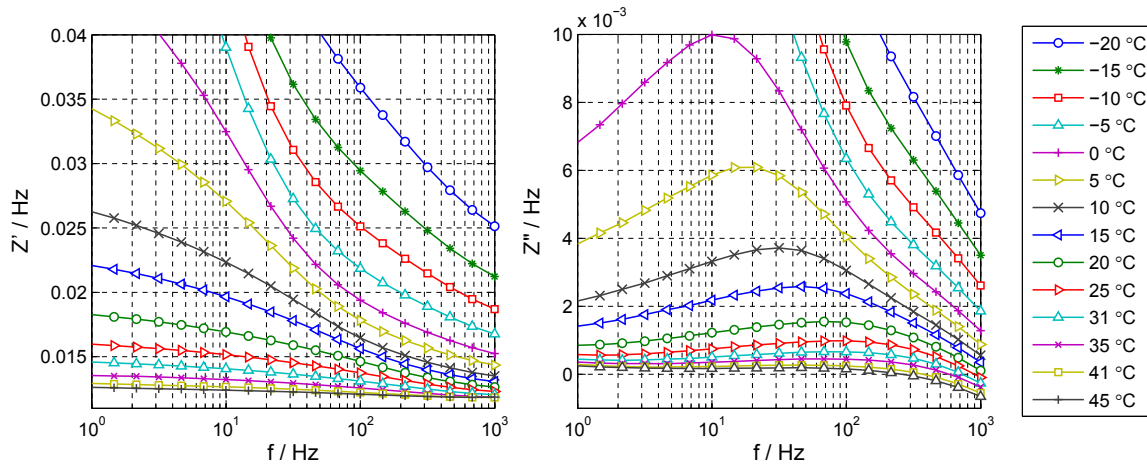

Fig. 6. Bode plot of Z' (left) and Z'' (right) at 50% SOC at various temperatures over the frequency range 1 Hz–2 kHz.

the values of a, b and c used in Eq. (7), to relate admittance to temperature.

4.2. Validation

Fig. 9(a) displays the results of the current pulse validation experiments, including (1) the surface and core temperature measurements T_{surf} and T_{core}, (2) the equivalent uniform cell temperature inferred from the impedance measurement alone $T_{uniform}$, and (3) the predicted core temperature $T_{max,est}$ — identified by combining the impedance and surface temperature measurements using the proposed model. Under 10 A pulses the difference between estimated and measured core temperature lies within 0.4 °C at all times, and under 20 A pulses the difference lies within 0.9 °C.

The performance of the model for a HEV drive cycle is investigated in a similar manner (Fig. 9(b)). The predicted maximum temperature shows good agreement with the measured core temperature, with a mean absolute error, $|\varepsilon|_{mean}$, of 0.6 °C (3% of the total core temperature increase from 8 °C to 28 °C). In contrast, if the temperature of the cell is assumed uniform (as in previous studies [12,13]), and $T_{uniform}$ equated to a uniform jelly roll temperature, then the maximum temperature of the cell is consistently

underestimated and $|\varepsilon|_{mean}$ is 2.6 °C (13% of the total core temperature increase from 8 °C to 28 °C). Fig. 10 shows the absolute error distributions for the each of these two cases, along with the mean and maximum errors and standard deviation in each case.
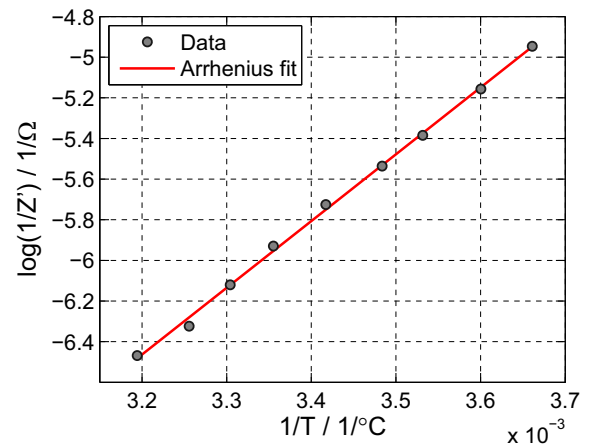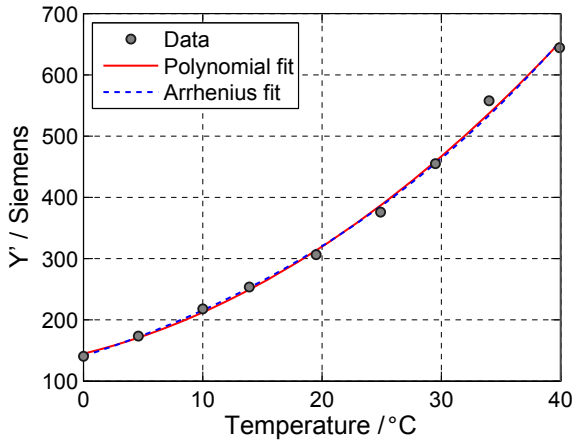

Fig. 7. Arrhenius fit to the measured impedance (at $f = 215$ Hz and SOC = 50%), accounting for the constant resistance of the current collector.

Fig. 8. Comparison of different fits to the experimental admittance vs. temperature data. Directly fitting a 2nd order polynomial to the admittance (blue line) gives approximately equivalent results to the Arrhenius fit of the impedance from Fig. 7 (green line with triangles). (For interpretation of the references to colour in this figure legend, the reader is referred to the web version of this article).

These plots reinforce the earlier assertion that failing to account for temperature non-uniformity results in consistent underestimation of the core temperature. Also, Fig. 10(a) shows that the error introduced by the steady state assumption discussed in Section 2.2, is relatively small in the studied drive cycle.
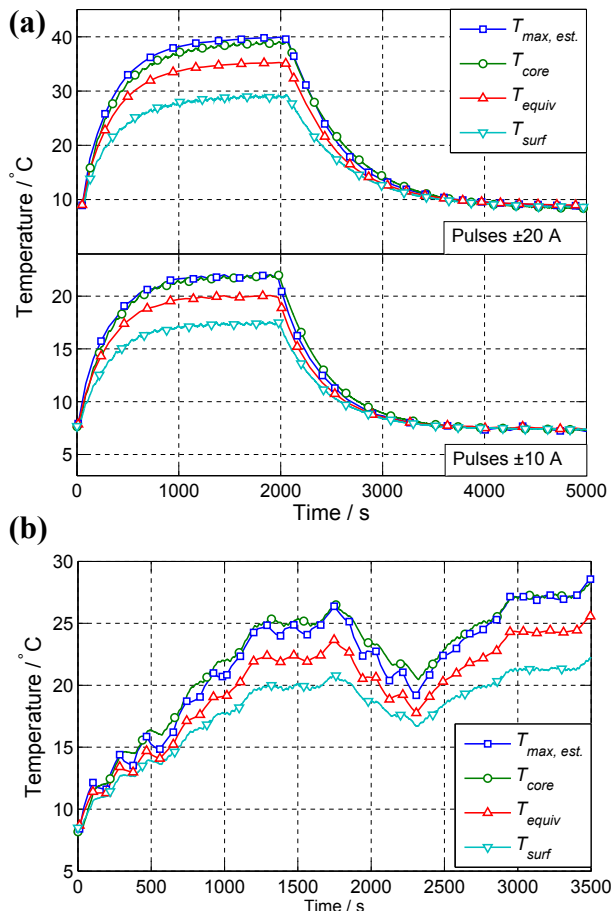
Fig. 9. Validation experiments results: (a) current pulses and (b) Artemis drive cycle.
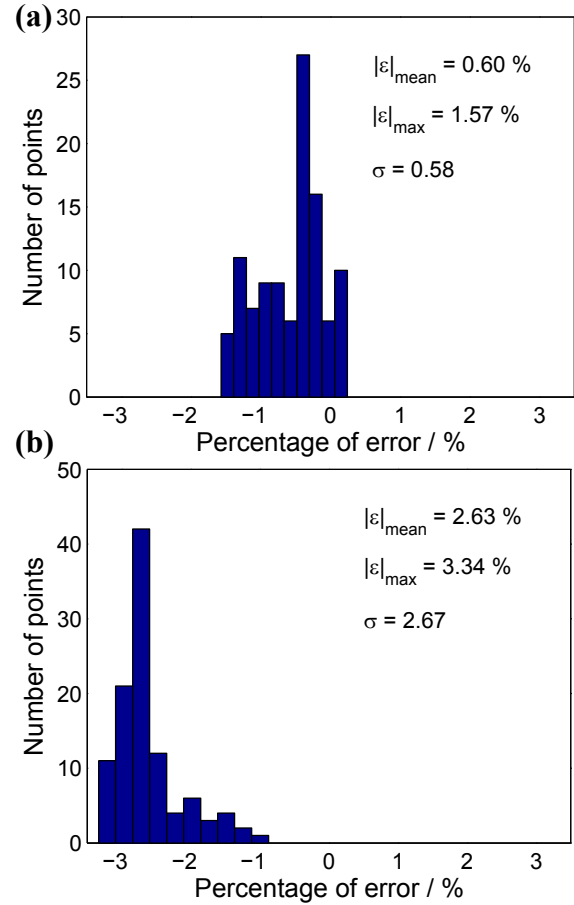
Fig. 10. Artemis drive cycle error analysis. (a) $\varepsilon = T_{core} - T_{max,est.}$; (b) $\varepsilon = T_{core} - T_{uniform}$

5. Conclusions

Knowledge of the internal temperature distribution of lithium-ion cells during operation is of paramount importance for safety and control purposes. This paper introduces a promising new approach for estimating the internal temperature distribution in cylindrical cells by combining measured electrochemical imped-ance and surface temperature. By treating the cell as a series of infinitesimal concentric annuli electrically connected in parallel, an analytical solution for the temperature distribution is obtained, using inputs of cell impedance at a single frequency and surface temperature. The model does not rely on knowledge of the cell thermal properties, heat generation rates or thermal boundary conditions, and it is efficient enough to be implemented in the BMS of an electric vehicle. The model is validated using internal ther-mocouple measurements, which has not previously been demon-strated for impedance-based temperature estimation.

Whilst this work shows that the method has promise, it also highlights a number of outstanding issues worthy of investigation. In particular, interpreting impedance measurements under super-imposed DC currents is yet to be systematically investigated. Also, the impact of non-constant environmental temperature could be investigated. Further work is also required to bring impedance measurement from the lab to online applications. Whilst ap-proaches capable of measuring impedance spectra across multiple frequencies using existing power electronics in a vehicle have already been developed [21,22], the use of such systems for online temperature measurement has yet to be demonstrated. The tech-nique proposed here requires a temperature sensor to be placed on

every cell and the impedance of each cell to be measured. This could be onerous for a large pack containing many cells, although for some high performance applications it may be justified, particularly when the alternative is to embed small temperature sensors in each cell. Whilst these issues remain challenging, ultimately this approach has the potential to provide fast, robust temperature estimation.

Acknowledgements

Nomenclature

c_p	specific heat capacity [J kg^{-1} K^{-1}]
E_a	activation energy [J]
f	frequency [Hz]
g	admittivity [S°m^{-1}]
g'	real admittivity [S m^{-1}]
g''	imaginary admittivity [S m^{-1}]
G	admittance [S]
G'	real admittance [S]
G''	imaginary admittance [S]
$\bar{I}$	current [A]
j	imaginary number
L	cell length [m]
$\dot{q}$	heat generation [W m^{-3}]
r	radial coordinate [m]
r_1	inner radius [m]
r_2	outer radius [m]
R	Universal gas constant [J K^{-1} mol^{-1}]
R_e	internal electrical resistance [Ω]
t	time [s]
T	temperature [K]
T_i	temperature at inner surface [K]
T_o	temperature at outer surface [K]
T_{surf}	measured temperature at outer surface [K]
T_{core}	measured temperature in core [K]
$T_{max,est.}$	maximum temperature estimated by model [K]
$T_{uniform}$	uniform cell temperature that would give rise to measured impedance [K]
U	voltage [V]
V	cell volume [m^3]
z	axial coordinate [m]
Z	impedance [Ω]
Z'	real impedance [Ω]
Z''	imaginary impedance [Ω]

Greek symbols

$\lvert\varepsilon\rvert_{mean}$	mean absolute error [K]
ε_{max}	maximum error [K]
ρ	density [kg m^{-3}]
σ	standard deviation
ω	frequency [rad]

Glossary

BMS	battery management system
EIS	electrochemical impedance spectroscopy
GEIS	galvanostatic electrochemical impedance spectroscopy
SOC	state of charge
SOH	state of health

References

[1] C. Forgez, D. Vinh Do, G. Friedrich, M. Morcrette, C. Delacourt, J. Power Sources 195 (2010) 2961–2968.

[2] Q. Wang, P. Ping, X. Zhao, G. Chu, J. Sun, C. Chen, J. Power Sources 208 (2012) 210–224.

[3] X. Lin, H.E. Perez, J.B. Siegel, A.G. Stefanopoulou, Y. Ding, M.P. Castanier, in: Les Rencontres Scientifiques d'IFP Energies nouvelles, Rueil-Malmaison, 6th–7th December, 2011.

[4] X. Lin, H.E. Perez, J.B. Siegel, A.G. Stefanopoulou, Y. Li, R.D. Anderson, Y. Ding, M.P. Castanier, IEEE Trans. Control Syst. Technol. 21 (2013) 1745–1755.

[5] X. Lin, H.E. Perez, S. Mohan, J.B. Siegel, A.G. Stefanopoulou, Y. Ding, M.P. Castanier, J. Power Sources 257 (2014) 1–11.

[6] Y. Kim, J.B. Siegel, A.G. Stefanopoulou, in: Am. Control Conf. (ACC), 2013, pp. 698–703. Washington DC, 2013.

[7] Y. Kim, S. Mohan, J.B. Siegel, A.G. Stefanopoulou, Y. Ding, in: 52nd IEEE Conference on Decision and Control, 2013, pp. 5680–5685. Florence, Italy.

[8] T.M. Bandhauer, S. Garimella, T.F. Fuller, J. Electrochem. Soc. 158 (2011) R1–R25.

[9] S. Santhanagopalan, P. Ramadass, J. (Zhengming) Zhang, J. Power Sources 194 (2009) 550–557.

[10] Z. Li, J. Zhang, B. Wu, J. Huang, Z. Nie, Y. Sun, F. An, N. Wu, J. Power Sources 241 (2013) 536–553.

[11] M.S.K. Mutyala, J. Zhao, J. Li, H. Pan, C. Yuan, X. Li, J. Power Sources 260 (2014) 43–49.

[12] R. Srinivasan, B.G. Carkhuff, M.H. Butler, A.C. Baisden, Electrochim. Acta 56 (2011) 6198–6204.

[13] R. Srinivasan, J. Power Sources 198 (2012) 351–358.

[14] Y. Troxler, B. Wu, M. Marinescu, V. Yufit, Y. Patel, A.J. Marquis, N.P. Brandon, G.J. Offer, J. Power Sources 247 (2014) 1018–1025.

[15] J.P. Schmidt, S. Arnold, A. Loges, D. Werner, T. Wetzel, E. Ivers-Tiffée, J. Power Sources 243 (2013) 110–117.

[16] L.H.J. Raijmakers, D.L. Danilov, J.P.M. van Lammeren, M.J.G. Lammers, P.H.L. Notten, J. Power Sources 247 (2014) 539–544.

[17] M. Fleckenstein, S. Fischer, O. Bohlen, B. Bäker, J. Power Sources 223 (2013) 259–267.

[18] M. Fleckenstein, O. Bohlen, M. a. Roscher, B. Bäker, J. Power Sources 196 (2011) 4769–4778.

[19] F.P. Incropera, D.P. De Witt, Fundamentals of Heat and Mass Transfer, sixth ed., 1985.

[20] B.V. Ratnakumar, M.C. Smart, L.D. Whitcanack, R.C. Ewell, J. Power Sources 159 (2006) 1428–1439.

[21] N.P. Brandon, D.A. Howey, P.D. Mitcheson, G. Offer, V. Yufit, IEEE Trans. Veh. Technol. 99 (2013) 1–10.

[22] N. Brandon, P. Mitcheson, D.A. Howey, V. Yufit, G.J. Offer, Battery Monitoring in Electric Vehicles, Hybrid Vehicles and Other Applications, 2012. US 13/819,305.